Scanning Tunneling Microscopy, Orbital-Mediated Tunneling Spectroscopy, and Ultraviolet Photoelectron Spectroscopy of Metal(II) Tetraphenylporphyrins Deposited from Vapor

L. Scudiero, Dan E. Barlow, Ursula Mazur, and K. W. Hipps*

Contribution from the Department of Chemistry and Materials Science Program, Washington State University, Pullman, Washington 99164-4630

Received January 8, 2001

Abstract: Thin films of vapor-deposited Ni(II) and Co(II) complexes of tetraphenylporphyrin (NiTPP and CoTPP) were studied supported on gold and embedded in Al−Al_2O_3−MTPP−Pb tunnel diodes, where M = Ni or Co. Thin films deposited onto polycrystalline gold were analyzed by ultraviolet photoelectron spectroscopy (UPS) using He I radiation. Scanning tunneling microscopy (STM) and orbital-mediated tunneling spectroscopy (STM−OMTS) were performed on submonolayer films of CoTPP and NiTPP supported on Au(111). Inelastic electron tunneling spectroscopy (IETS) and OMTS were measured in conventional tunnel diode structures. The highest occupied π molecular orbital of the porphyrin ring was seen in both STM−OMTS and UPS at about 6.4 eV below the vacuum level. The lowest unoccupied π* molecular orbital of the porphyrin ring was observed by STM−OMTS and by IETS−OMTS to be located near 3.4 eV below the vacuum level. The OMTS spectra of CoTPP had a band near 5.2 eV (below the vacuum level) that was attributed to transient oxidation of the central Co(II) ion. That is, it is due to electron OMT via the half-filled d_{z^2} orbital present in Co(II) of CoTPP. The NiTPP OMTS spectra show no such band, consistent with the known difficulty of oxidation of the Ni(II) ion. The STM-based OMTS allowed these two porphyrin complexes to be easily distinguished. The present work is the first report of the observation of STM−OMTS, tunnel junction OMTS, and UPS of the same compounds. Scanning tunneling microscope-based orbital-mediated tunneling provides more information than UPS or tunnel junction-based OMTS and does so with molecular-scale resolution.

Introduction

Metalloporphyrins are intensively studied for many reasons. They play an important role in a wide variety of biological processes ranging from oxygen transport to pigmentation changes. They can act as catalysts,[1] and there has been significant recent interest in structural distortions from planar geometry.[2−4] Metalloporphyrins can undergo reversible redox reactions in which the site of electron transfer may be localized on the porphyrin ring or on the central metal ion. Both reaction types are important in natural processes.[5] Thin porphyrin films on metal and semiconductor surfaces are also of great interest. Chemical sensors made from porphyrin films have been reported.[6] In the electrochemical environment, infrared (IR) spectroscopy,[5] Raman spectroscopy,[7] and scanning tunneling microscopy (STM)[8−15] studies have provided a wealth of information on the structure of the porphyrin at the electrode surface. Langmuir−Blodgett films,[16] self-assembled monolayers,[8,17] and self-organized structures[18,19] of porphyrins have been studied by a wide variety of techniques. Vapor-deposited porphyrins have received much less attention.

IR transmission spectra and electron diffraction studies have been performed on thin films of metal-free tetraphenylporphyrin (H_2TPP) vapor deposited onto KCl.[20] Ultra-high-vacuum (UHV) studies of vapor-deposited copper(II) tetrakis(3,5-di-*tert*-butylphenyl)porphyrin (CuTTBPP) on Cu(100) have been reported

* To whom correspondence should be addressed. E-mail: hipps@wsu.edu.

(1) Collman, J. P.; Halbert, T. R.; Suslick, K. S. In *Metal Ions in Biology*; Spiro, T. G., Ed.; Wiley: New York, 1980; Vol. 2, p 1.
(2) Unger, E.; Beck, M.; Lipski, R.; Dreybodt, W.; Medforth, C. J.; Smith, K.; Schweitzer-Stenner, R. *J. Phys. Chem. B* **1999**, *103*, 10022.
(3) Piffat, C.; Melamed, D.; Spiro, G. *J. Phys. Chem*. **1993**, *97*, 7441.
(4) Jentzen, W.; Unger, E.; Song, X.; Jia, S.; Tyek, I. T.; Stenner, R. S.; Draybrodt, W.; Scheidt, W. R.; Shelnutt, J. A. *J. Phys. Chem. A* **1997**, *101*, 5789.
(5) Jones, D.; Hinman, A. S. *J. Chem. Soc., Dalton Trans.* **1992**, 1503.
(6) Paolesse, R.; Di Natale, C.; Dall'Orto, V.; Macagnano, A.; Angelaccio, A.; Motta, N.; Sgarlata, A.; Hurst, J.; Rezzano, I.; Mascini, M.; D'Amico, A.; *Thin Solid Films* **1999**, *354*, 245.
(7) Atamian, M.; Donohoe, R. J.; Lindsey, J. S.; Bocian, D. F. *J. Phys. Chem.* **1989**, *93*, 2236.
(8) Duong, B.; Arechabaleta, R.; Tao, N. J. *J. Electroanal. Chem.* **1998**, *447*, 63.
(9) Kuniatke, M.; Batina, N.; Itaya, K. *Langmuir* **1995**, *11*, 2337.
(10) Ogaki, K.; Batina, N.; Kuniake, M.; Itaya, K. *J. Phys. Chem.* **1996**, *100*, 7185.
(11) Kunitake, M.; Akiba, U.; Batina, N.; Itaya, K. *Langmuir* **1997**, *13*, 1607.
(12) Ogaki, K.; Batina, N.; Kunitake, M.; Itaya, K. *J. Phys. Chem.* **1996,** *100*, 7185.
(13) Han, W.; Durantini, E. N.; Moore, T. A.; Moore, A. L.; Gust, D.; Rez, P.; Letherman, G.; Seely, G.; Tao, N.; Lindsay, S. M. *J. Phys. Chem. B* **1997**, *101*, 10719.
(14) Tao, N. J. *Phys. Rev. Lett.* **1996**, *76*, 4066.
(15) Tao, N. J.; Cardenas, G.; Cunha, F.; Shi, Z. *Langmuir* **1995**, *11*, 4445.
(16) Palacin, S.; Ruaudel-Teixier, A.; Barraud, A. *J. Phys. Chem.* **1986**, *90*, 6237.
(17) Shimazu, K.; Takechi, M.; Fugii, H.; Suzuki, M.; Saiki, H.; Yoshimura, T.; Uosaki, K. *Thin Solid Films* **1996**, *273*, 250.
(18) Thomas, P.; Berovic, N.; Laitenberger, P.; Palmer, R.; Bampos, N.; Sanders, J. *Chem. Phys. Lett.* **1998**, *294*, 229.
(19) Furukawa, M.; Tanaka, H.; Sugiura, K.; Sakata, Y.; Kawai, T. *Surf. Sci.* **2000**, *445*, L58.
(20) Yangi, H.; Ashida, M.; Harima, Y.; Yamashita, K. *Chem. Lett.* **1990**, 385.

10.1021/ja0100726 CCC: $20.00
Published on Web 03/29/2001

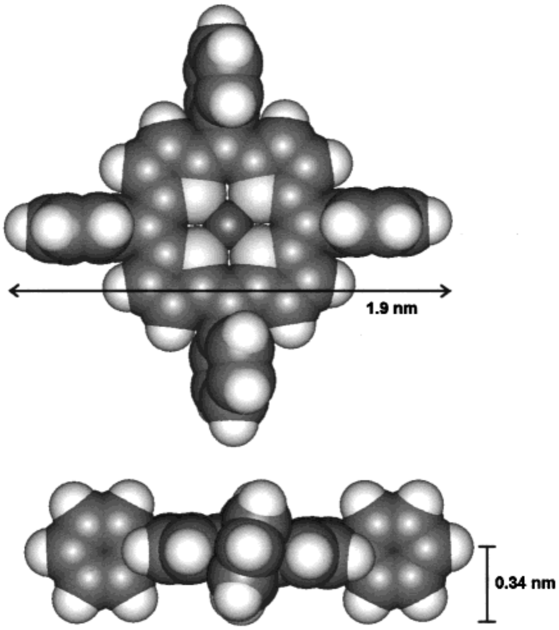

Figure 1. CPK model of a typical metal(II)TPP. The four nitrogens that bind the central metal ion are shown in light gray. The molecule is shown both in top and side views so that the orientation of the phenyl rings relative to the porphyrin ring may be seen.

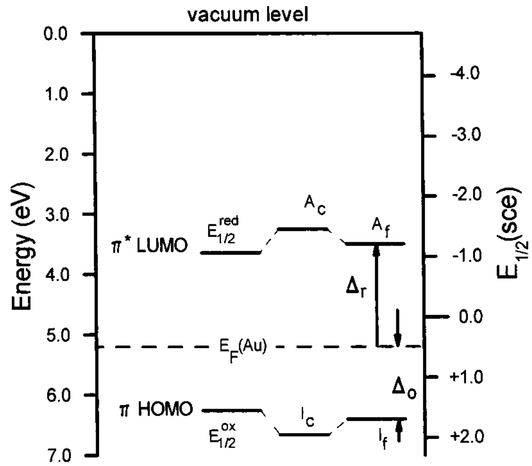

Figure 2. Schematic of critical energy levels of a porphyrin relative to the vacuum level, saturated calomel electrode, and Fermi energy. In the case of CoTPP, there is an additional active level just below E_F(Au), the $d_{z^2}^1$-to-$d_{z^2}^0$ ionization. A_c and A_f are electron affinity levels for crystalline and for thin film on metal phases, respectively. A is the energy required to take an electron from a negative ion state to the vacuum level and leave a neutral molecule. I_c and I_f are the corresponding ionization energies and are the energies required to take an electron from an orbital of a neutral molecule to the vacuum level.

by Gimzewski,[21,22] who has also provided a single image of a mixed monolayer of CuTPP and CuTTBPP on Cu(100).[22] Recently, Scudiero et al. reported an X-ray photoelectron spectroscopy (XPS), IR, and STM study of submonolayer films of CoTPP, NiTPP, and CuTPP on Au(111) under UHV conditions.[23]

Scudiero et al. analyzed IR and XPS spectra of thin films of Co(II)TPP, Cu(II)TPP, and Ni(II)TPP in terms of oxidation state, chemical composition, and orientation.[23] It was found that these compounds may be thermally deposited onto gold without changes in chemical composition or oxidation state. Molecular resolution STM images were reported, and chemical specificity in STM imaging for these complexes was demonstrated.[23] As had been previously shown for metal phthalocyanine (MPc) complexes,[24−26] varying the metal ion at the center of a metal(II) tetraphenylporphyrin (MTPP) produced huge variations in the constant current STM images.[23] This was interpreted to indicate large changes in tunneling probability associated with occupancy of the d_{z^2} orbital of the transition metal ion. A space-filling model (CPK) of a typical first-row M(II)TPP is shown in Figure 1 as both a top view and a side view.

In the present article we focus on the electronic spectroscopic properties of metallotetraphenylporphyrins. In particular, we determine the energies of the highest occupied and lowest unoccupied π orbitals and the highest occupied d metal orbital. Results from STM, tunnel diode, and ultraviolet photoelectron spectroscopy (UPS) measurements overlap and agree in their regions of overlap. The electrochemical model for estimating orbital-mediated tunneling bands is found to give good qualitative agreement with experiment, and good quantitative agreement for transient reduction processes and oxidative processes near the Fermi energy, E_F. The quantitative predictions of the model are poor for oxidative processes far from E_F.

To contrast and compare these disparate experimental results (inelastic electron tunneling spectroscopy (IETS), STM, orbital-mediated tunneling spectroscopy (OMTS), UPS, and electrochemistry), we will utilize the energy of the vacuum level (zero kinetic energy electron) as a unifying reference point. IETS and STM−scanning tunneling spectroscopy (STS) data are conventionally presented with the zero taken at the Fermi level, E_F, and peak positions are reported as shifts (Δ_o and Δ_r). Once E_F is determined, however, these can be converted to energies below the vacuum level, as shown in Figure 2. Similarly, ultraviolet photoelectron spectroscopic determination of occupied orbital energies is normally done relative to the Fermi energy, and these binding energies can also be converted (using Figure 2) into ionization energies, I (orbital energies below the vacuum level). Electron affinities, A, the energy gained by adding an electron to an unoccupied orbital, are conventionally given relative to the vacuum level. Reduction and oxidation potentials, often given relative to a saturated calomel electrode (SCE), may also be converted to energies below the vacuum level by using a procedure reported by Richardson.[27] Key to many of these conversions is a knowledge of the Fermi energy relative to the vacuum level. Thus, ultraviolet photoelectron spectroscopy will first be used to determine the Fermi energies of the Au(111) and polycrystalline gold substrates used. These Fermi energies will then be used to convert the variously measured quantities to energies below the vacuum level.

Experimental Section

Materials. Metalloporphyrins were purchased from Porphyrin Products and used as supplied. Gold, lead, and aluminum metals were >99.99% purity. The porphyrins were deposited from Ta metal sources for all STM and UPS samples, while a quartz crucible was used for the IETS films.

STM Sample Preparation and Data Acquisition. Epitaxial Au(111) films with well-defined terraces and single atomic steps were

(21) Jung, T. A.; Schlittler, R. R.; Gimzewski, J. K.; Tang, H.; Joachim, C. *Science* **1996**, *271*, 181.
(22) Gimzewski, J. K.; Jung, T. A.; Cuberes, M. T.; Schlittler, R. R. *Surf. Sci.* **1997**, *386*, 101.
(23) Scudiero, L.; Barlow, D. E.; Hipps, K. W. *J. Phys. Chem. B* **2000**, *104*, 11899−11905.
(24) Lu, X.; Hipps, K. W. *J Phys. Chem. B* **1997**, *101*, 5391.
(25) Lu, X.; Hipps, K. W.; Wang, X. D.; Mazur, U. *J. Am. Chem. Soc.* **1996**, *118*, 7197.
(26) Barlow, D.; Hipps, K. W. *J. Phys. Chem. B* **2000**, *104*, 2444.
(27) Richardson, D. E. *Inorg. Chem.* **1990**, *29*, 3213.

prepared on mica by previously described methods.[24,26] These films were 0.1−0.2 μm thick and had a mean single grain diameter of about 0.5 μm. Unlike true single-crystal gold,[28] these small crystal grains showed reconstruction line spacing ranging from 6.3 to about 9.0 nm. The gold films were transferred via air-lock into the UHV STM chamber (working pressure $\sim 8 \times 10^{-10}$ Torr), where the MTPP compounds were deposited and then studied without exposure to air. The thickness of the MTPP layers was determined with a quartz crystal thin-film monitor. The deposition rates used were so low (<0.01 nm/s) that there is significant uncertainty in the reported thickness, perhaps as much as a factor of 2. The STM head used was produced by McAllister Technical Services (Coeur d'Alene, ID) and is of the inertial approach type. A Digital Instruments Nanoscope III controller was used to acquire and process the reported data. Constant current images are reported, and any filtering is indicated in the appropriate figure caption. All images were acquired at about 21 °C. Both etched W and cut $Pt_{0.8}Ir_{0.2}$ tips were used. Generally, the tips required a UHV cleaning step (electron beam bombardment) in order to produce high-quality images. Spectroscopy was performed by measuring d*I*/d*V* as a function of *V* at a fixed tip−sample separation (feed back off). Digital Instruments software was used to collect d*I*/d*V* spectra both with modulation turned on (50−100 mV) and with modulation off. The resulting spectra were qualitatively the same, but the results were less noisy when modulation was used. The d*I*/d*V* data presented here are the average of 8−12 spectra. Scanning tunneling spectra (d*I*/d*V* at fixed height) were measured both on the islands of MTPP and over the clean gold surface as pairs. Spectra having anomalous structures over gold indicated that tip artifacts were present, and both the MTPP and the Au surface d*I*/d*V* curves were discarded. The d*I*/d*V* curves measured in the STM environment can be related to the normalized tunneling intensities (NTIs) measured in the tunnel diode environment.[29] While the OMTS bands appear as peaks in d*I*/d*V*, they are distorted derivative features in the NTI spectra normally reported from tunnel junctions.

Tunnel Junction Preparation and Data Acquisition. $Al-Al_2O_3-$MTPP−Pb tunnel diodes were fabricated by the same methods that were employed for other OMTS studies.[30] The CoTPP and NiTPP were spin-doped from benzene solutions of concentration 0.3−0.5 g/L.[31,32] Tunneling spectra were collected as normalized tunneling intensities (NTI) versus *V*, which are equivalent to $|(d\sigma/dV)/\sigma|$ versus *V*.[33,34] The NTI spectra were measured at 4 and 77 K by immersing the completed and wired junctions in liquid helium or liquid nitrogen, respectively. A modulation voltage of 4 mV rms was used, and all spectra are the sum of more than 64 scans. A low-order polynomial (less than fifth order) was fit to selected regions of the raw data, and this polynomial was subtracted from the entire NTI curve. The Fermi energy of the tunnel junction environment was taken as 4.3 eV below the vacuum level.

UPS Sample Preparation and Data Acquisition. UPS data were obtained with a homemade He lamp source which produces two resonance lines, He I (21.2 eV) and He II (40.8 eV), by cold cathode capillary discharge. The He lamp was set to run with a filament current of 17 A and a voltage of 9 V and He gas pressure at 250 mT. The discharge was adjusted to 190 V and 0.5 A. Only the 21.2 eV He I line was used in this study. A platinum-coated concave 600 groove/mm reflection grating with a 3.5° blaze angle coupled with a gold-coated spherical focusing mirror was used to produce monochromatic UV radiation. The base pressure in the monochromator chamber was 2×10^{-9} Torr. The UPS system is attached via a UHV valve to a Kratos Axis-165 electron spectrometer having a base pressure of 5×10^{-10} Torr.

Two different types of gold surfaces were studied: Au(111) samples (140 nm thick) made in a vacuum ($<3 \times 10^{-9}$ Torr) by vapor deposition on mica[35] and polycrystalline Au foil (99.985% purity). The gold foil was cleaned by heating and argon ion etching before use. The Au(111) samples were prepared exactly as described above for the STM substrates. Both types of gold were used to check the substrate work function and the calibration of the He lamp. In addition, the polycrystalline gold sample was used as the substrate for the MTPP UPS studies. NiTPP and CoTPP were thermally deposited onto polycrystalline gold, in a vacuum (5×10^{-9} Torr) prep chamber attached to the UPS spectrometer. The thickness of the samples was 4 nm, as determined with a quartz crystal microbalance and using a density of 1.2 g/cm^3.

The ultraviolet photoelectron spectra were acquired using an electrostatic lens that focused the ejected electrons into the spectrometer. A bias of −20 V was applied to the sample to shift the spectra out of the nonlinear region of the analyzer (KE = 0−10 eV). The spectrometer was used in fixed analyzer transmission mode with a pass energy of 20 eV and spatial resolution of 120 μm. The photoemitted electron energies were analyzed by a Kratos hemispherical analyzer and counted by eight channel electron multipliers. Under these conditions, the energy resolution of the spectrometer is better than 150 meV, which was determined at the Fermi edge of an Ar-etched single crystal of Au(111).

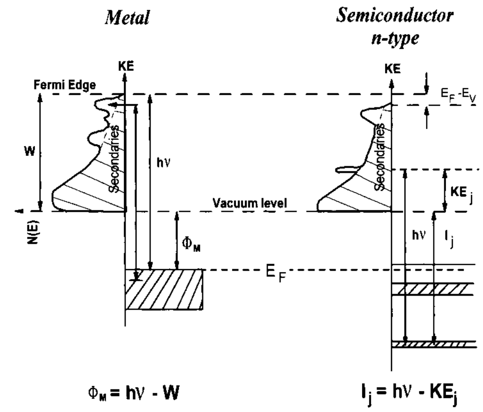

Figure 3. Schematic representation of ultraviolet photoelectron emission for the case of a metal and a type n semiconductor.

Results and Discussion

Ultraviolet Photoemission Spectroscopy. In general, the photoemission process is described by the following expression:

$$M_0 + h\nu \rightarrow M_j^+ + e^-$$

The ionization energy to produce state *j* of the positive ion, M^+, is expressed by

$$I_j = h\nu - KE_j \tag{1}$$

where *I* is the ionization energy measured relative to the vacuum level, KE is the kinetic energy of the ejected photoelectron, and $h\nu$ is the energy of the photon. Often, because of experimental convenience, UPS spectra are reported as binding energies relative to the Fermi energy.

Figure 3 shows a band diagram for metals and semiconductors (n-type) that illustrates how a UPS spectrum is generated. A sample is placed in UHV and irradiated with UV light, electrons are ejected from the higher bands, and their kinetic energy is measured. UPS probes the highest occupied orbitals at higher resolution (typically <150 meV) than is possible with XPS (≥0.55 eV). Because the photoelectrons emitted in the case of UPS have much smaller KE (∼20 eV) than those associated with valence band XPS (∼1400 eV), UPS is more surface

(28) Barth, J. V.; Brune, H.; Ertl, G.; Behm, R. J. *Phys. Rev. B* **1990**, *42*, 9307.
(29) Hipps, K. W.; Mazur, U. *J. Phys. Chem. B* **2000**, *104*, 4707−4710.
(30) Mazur, U.; Hipps, K. W. *J. Phys. Chem. B* **1999**, *103*, 9721−9727
(31) Hipps, K. W.; Mazur, U. *J. Phys. Chem.* **1993**, *97*, 7803−7814.
(32) Mazur, U.; Hipps, K. W. *J. Phys. Chem.* **1994**, *98*, 5824−5829.
(33) Hipps, K. W.; Mazur, U. *Rev. Sci. Instrum.* **1988**, *59*, 1903−1905.
(34) Seman, T. R.; Mallik, R. R. *Rev. Sci. Instrum.* **1999**, *70*, 2808−2814.

(35) Lu, X.; Hipps, K. W.; Wang, X. D.; Mazur, U. *J. Am. Chem. Soc.* **1996**, *118*, 7197.

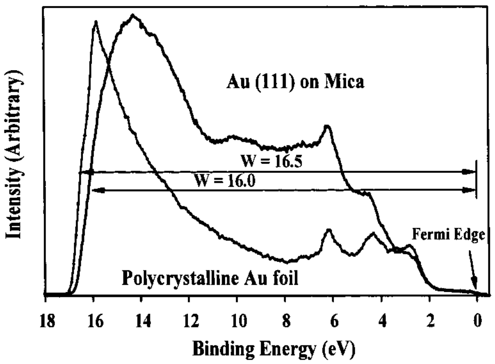

Figure 4. Raw UPS data obtained from thin-film Au(111) and from polycrystalline gold foil. Binding energies are given relative to the Fermi energy.

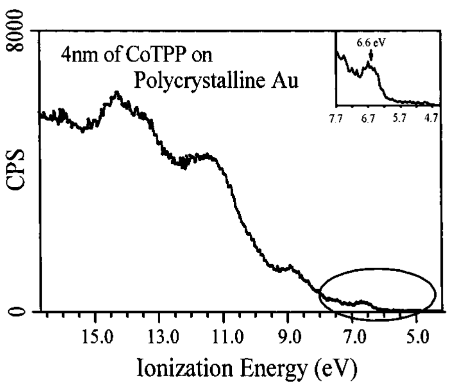

Figure 5. Raw UPS data obtained from a 4 nm film of CoTPP vapor deposited on a clean polycrystalline gold surface. The inset shows the highest occupied π orbital band in more detail.

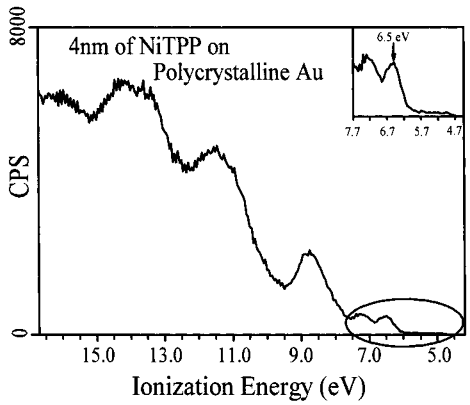

Figure 6. Raw UPS data obtained from a 4 nm film of NiTPP vapor deposited on a clean polycrystalline gold surface. The inset shows the highest occupied π orbital band in more detail.

Table 1. Ionization Energy Values Obtained from 4 nm Thick Films of NiTPP and CoTPP Deposited on Polycrystalline Au and Also from the Vapor Phase

compound	binding energy of UPS bands (eV)						
CoTPP (4 nm)[a]	6.6		8.8	11.4	13.4	14.2	16.0
NiTPP (4 nm)[a]	6.5	7.2	8.7	11.4	13.5	14.2	18.0
NiTPP (vapor)[b]	6.44	7.21	8.02	11.72	13.77	14.54	
	6.62		8.92				
MnTPP (vapor)[b]	6.44		7.66	11.42	13.45	14.09	
	6.61		8.80				
H_2TPP (vapor)[b]	6.39		7.71	11.63	13.57	14.32	
	6.72		8.86				

[a] This work. MTPP deposited on polycrystalline gold. Work function taken as 4.7 eV. [b] Vapor phase data from ref 37. Values are relative to (below) the vacuum level.

sensitive than XPS. UPS is also more sensitive to p-type valence orbitals than d-type. Thus, valence shell UPS is the technique of choice for studying the highest energy π molecular orbitals of the metal TPP complexes.

Figure 4 displays the ultraviolet photoelectron spectra from both the thin-film Au(111) and the polycrystalline gold samples. We used Figure 4 and the equation for the work function, $\phi_M = 21.2 - W$ (for He I), to determine the work function, ϕ, of the thin-film Au(111) and the polycrystalline gold foil. These values were 5.20 ± 0.15 and 4.70 ± 0.15 eV, respectively. The value for the Au(111) film, 5.2 eV, is in good agreement with values found in the literature for Au(111).[36] These work function values were used to convert measured binding energies of MTPP films to vacuum-state referenced values.

Figures 5 and 6 provide the raw UPS data obtained from a 4 nm film of CoTPP and NiTPP, respectively, deposited onto polycrystalline gold. The *x*-axis is the binding energy relative to the vacuum level (ionization energy). The insets show the first few electronvolts of the spectrum in greater detail. Note that the NiTPP spectrum has a band near 7.2 eV that is either weaker or absent in the CoTPP spectrum. This extra band has also been observed in vapor-phase ultraviolet photoelectron spectra of NiTPP.[37] Table 1 contrasts the bands observed in our thin-film samples with those reported by Khandelwal and Roebber[37] for several metalloporphyrins in the vapor phase. Note that the vapor-phase spectra are better resolved and that the bands we see near 6.5 and 8.8 eV are actually each a doublet. Note also that (aside from the 7.2 eV band in the case of NiTPP) the observed ionization energies are only weakly dependent on the central metal and are thus assigned to occupied orbitals of the porphyrin ring or to those of the four phenyl groups. In fact, Battye et al.[38] have demonstrated that the valence band XPS spectra of both the metal phthalocyanines and the metal tetraphenylporphyrins can be reproduced well simply by adding the 8−30 eV XPS spectra of benzene and pyrrole, thereby showing that none of the features in that region are due to the central metal ion. The vapor-phase ultraviolet photoelectron spectrum of benzene in the 9−20 eV binding energy region (relative to E_F) is also remarkably similar to that of ZnTPP.[38] The highest occupied molecular orbitals (HOMOs) are the nearly degenerate $a_{1u}(\pi)$ and $a_{2u}(\pi)$ MOs of the porphine ring and are split by only 0.2−0.3 eV. Khandelwal and Roebber[37] assign the highest occupied MO to be the a_{2u} for CuTPP, ZnTPP, and MgTPP, but choose the a_{1u} for NiTPP on the basis of reported EPR and optical spectra. In our thin-film work, we always observe only one peak in this region of the spectrum.

STM Imaging. Figure 7 is a typical constant current image of NiTPP on Au(111) observed at low resolution. At this low resolution, the individual NiTPP molecules appear as dots making up well-defined, single-molecule-thick islands (e.g., region B). The regions between the islands (e.g., region A) appear to be uncovered Au(111) surfaces, and the $I-V$ curves obtained in these regions are similar to those from MTPP-free substrates. The large height step (feature C) along the right side of the figure is due to a monatomic step of the Au(111) substrate. One can also observe striations running through a portion of the NiTPP islands. These are due to reconstruction of the gold surface and appear as pairs of lines. Two pairs are marked by

(36) *CRC Handbook of Chemistry and Physics*, 70th ed., E93; CRC Press: Boca Raton, FL, 1989.

(37) Khandelwal, S. C.; Roebber, J. L. *Chem. Phys. Lett.* **1975**, *34*, 355−359.

(38) Battye, F. L.; Goldman, A.; Kasper, L. *Phys. Stat. Sol. B* **1977**, *80*, 425−432.

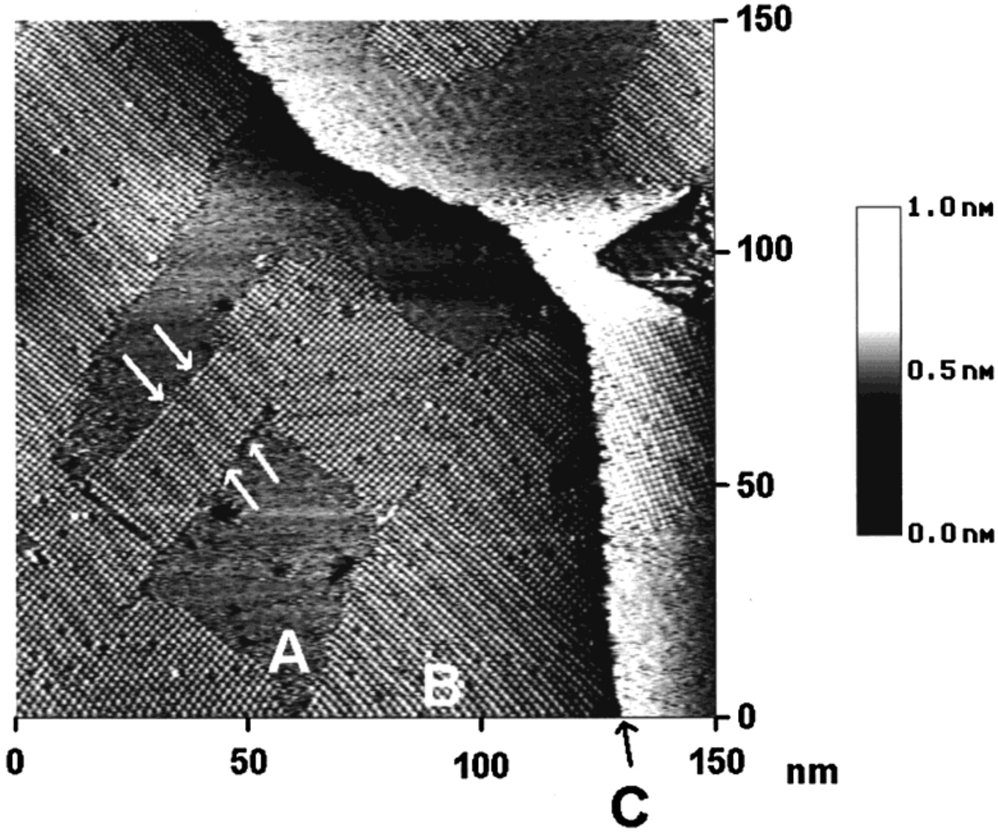

Figure 7. Typical constant current image of NiTPP on Au(111) observed at low resolution. The image was obtained with a PtIr tip at a sample bias voltage of −1.5 V and a set point of 300 pA. The image has been flattened. (Coverage about 0.3 monolayer.) The region marked A is uncovered Au(111), and the region marked B is a single-molecule-thick layer of NiTPP. The line marked C is a single gold atomic step, while the white arrows indicate pairs of reconstruction lines.

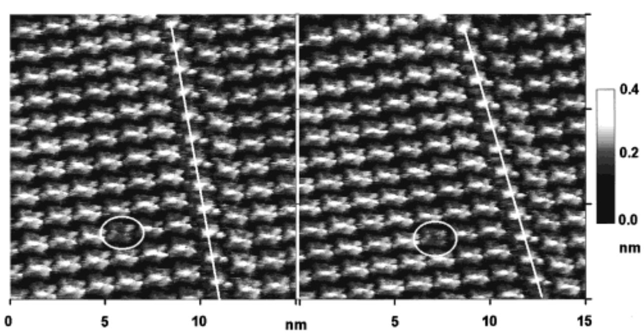

Figure 8. Medium-resolution constant current STM image of CoTPP at submonolayer coverage on Au(111). The image was acquired with a PtIr tip at 0.2 V bias, with a setpoint of 1.0 nA.

arrows in the figure. The small-grain gold films used in these studies (about 0.5 μm in diameter) generally have a larger reconstruction line spacing than seen on large single-crystal Au(111) surfaces. Unlike true single-crystal gold,[28] these small crystal grains show reconstruction line spacing ranging from 6.3 to about 9.0 nm. It should also be noted that adsorbed MTPP (both CoTPP and NiTPP) enhances the contrast associated with the reconstruction.

Figure 8 shows a pair of higher resolution images of CoTPP on Au(111). These images were taken sequentially in time, and the right image was acquired immediately after the left one. Figure 8 shows the four-fold symmetry expected for the molecule and the bright center associated with the central Co(II) ion. Similar resolution NiTPP images do not show a bright center. The difference in metal ion contrast has been explained in terms of occupation of the d_{z^2} orbital.[23−26] The d-orbital configuration of CoTPP is $d_{xz}^2 d_{yz}^2 d_{xy}^2 d_{z^2}^1$,[39] while NiTPP has a filled d_{z^2} orbital. This metal-ion-dependent contrast can be effectively used to study 2-D kinetics. In fact, this particular pair of images was chosen because of the presence of an impurity molecule (possibly H_2TPP) in this pair of images (see circled molecule in Figure 8). Another useful marker in Figure 8 is the grain boundary, indicated by a white line. Using these features as markers, it is easy to see that the sample is experiencing thermal drift, with the greatest motion being from left to right. This drift causes the CoTPP molecules to appear elongated relative to their actual four-fold symmetry, a result that is further exaggerated by a slightly elongated tip. The tip elongation can also be seen in the relative fast and slow scan direction molecular spacing. The left−right molecular separation appears smaller than the up−down separation.

IETS and OMTS. An energy level diagram and actual NTI data for the [Al−Al_2O_3−vanadyl pthalocyanine (VOPc)−Pb] tunnel junction are shown in Figure 9. This figure can be used to explain features observed in d*I*/d*V*−*V* and in NTI−*V* curves. Since more of the tunneling current comes from electrons near the Fermi surface, only those are considered in this cartoon of the process. When the bias voltage is low and there is no structured material in the barrier region, electrons can tunnel elastically across the barrier. This elastic current is nearly linear at low bias and becomes nonlinear at high bias. From past experience with IETS, it is known that both intense inelastic bands and OMTS bands generally are easily discernible in the *I*−*V* curve. If the tunneling electrons interact inelastically with the adsorbate, they lose the amount of energy necessary to excite

(39) Subramanian, J. In *Porphyrins and Metalloporphyrins*; Smith, K. M., Ed.; Elsevier Scientific: New York, 1975; p 568.

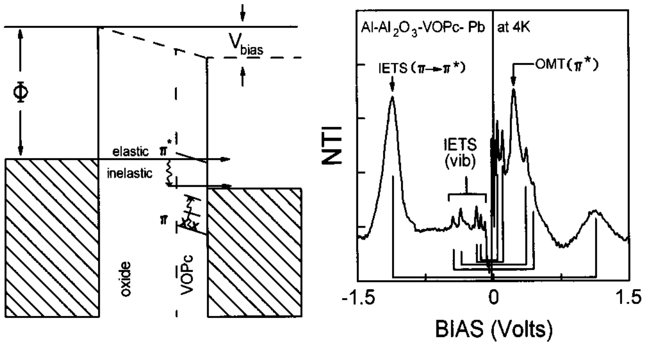

Figure 9. Schematic diagram of inelastic and resonant elastic tunneling processes (left). Tunneling spectroscopy data obtained from an Al−Al_2O_3−VOPc−Pb tunnel junction at 4 K, with 10 mV rms modulation (VOPc is vanadyl phthalocyanine). Vertical lines guide the eye to the inelastic excitations which occur in both bias directions. The OMTS band associated with transient reduction of the Pc ring, on the other hand, appears only on the Pb+ bias side. Reproduced with permission from ref 46. Copyright 2000 American Chemical Society.

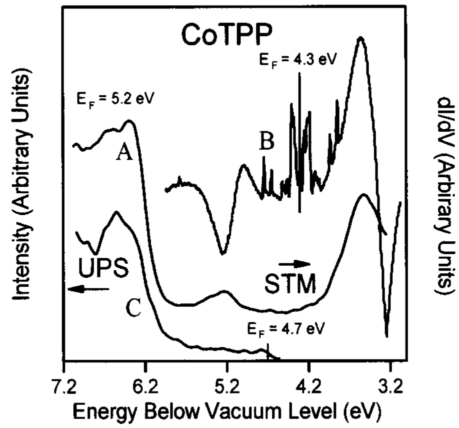

Figure 10. Combined results of UPS, STM d*I*/d*V* OMTS, and tunnel junction IETS and OMTS of CoTPP thin films. Curve positions on the *x*-axis are adjusted for differences in device work function. Trace A gives the STM d*I*/d*V* data. These were acquired from a 0.08 nm thick CoTPP film on Au(111) using a tungsten tip at a fixed height consistent with 0.3 nA and 0.3V bias. B is the NTI−*V* spectrum from an Al−Al_2O_3−CoTPP−Pb junction taken at 4 K, and C is the smoothed ultraviolet photoelectron spectrum of a 4 nm film on polycrystalline gold.

it (a vibrational mode excited by inelastic tunneling is shown on the left side of Figure 9) and proceed to tunnel out of the barrier. If the initial energy of the electron is insufficient to both excite the inelastic process and retain energy greater than the right-hand metal Fermi energy, the process is forbidden by the Pauli principle, because the final levels are fully occupied. Thus, there is an onset bias for the inelastic channel to contribute to the tunneling current. For a very intense inelastic electronic excitation, this produces a rounded step in the d*I*/d*V*−*V* curve and a strong peak in the NTI. Because these inelastic processes depend only on differences in electron energy, they occur in both bias directions, and the inelastic tunneling spectrum (IETS) should be similar in either bias.

For quasi-resonant tunneling, where the tunneling electron loses little or no net energy to the adsorbate, we would expect the d*I*/d*V* curve to reflect the density of states for the adsorbate (empty states in the case of this example). Thus, the NTI−*V* spectra would contain a derivative-like band, and a peak would appear in d*I*/d*V*−*V* spectra. The conceptual model for OMTS via a LUMO (unoccupied orbital) is shown by the schematic in Figure 9. As the potential across the junction becomes more positive, the Fermi energy of the left-hand metal comes into energetic resonance with the unoccupied MO. Provided the total gap length is large compared to the adsorbate thickness, a peak will be seen in the d*I*/d*V*−*V* curve at the energy of the LUMO.[29,40] Thus, the electron affinity of the adsorbate is equal to the work function of the right-hand metal minus the applied bias at which the peak in d*I*/d*V* occurs (see Figure 2). In reverse bias, the LUMO never comes into resonance with the Fermi energy, and no peak due to unoccupied orbitals is seen.[41,42] On the other hand, occupied orbitals can be brought into resonance with the left-hand metal Fermi surface only when an appropriate negative bias is applied. *Thus, both occupied and unoccupied orbitals can be probed by OMTS.* When NTI−*V* spectra are collected, OMTS is easy to identify because, unlike the IETS bands, the OMTS is expected to be highly bias asymmetrical and derivative-like in shape. That is, the IETS peaks appear at both positive and negative bias as Gaussian-like peaks, while the OMTS bands appear in only one polarity and are differential in shape. In NTI spectra, the differential OMT bands have an identifiable peak occurring somewhat below the maximum in d*I*/d*V*—the shift is approximately 0.1 V, which is of the order of the half-width of the OMT peak seen in the NTI spectrum at an amplitude of 1/e of its maximum value.[29] Taking the work function of Pb to be 4.3 eV[43] and the position of the OMTS peak in Figure 9 to be 0.23 eV, and adding 0.08 eV (the 1/e half-width of the peak), one obtains an electron affinity of 4.0 eV.

Turning next to the STM d*I*/d*V* spectra, OMTS is present as simple peaks, the band maxima of which correspond to orbital positions relative to the Fermi energy (at Δ_r and Δ_o relative to E_F in Figure 2). When the sample or the tip, or both, are at room temperature, the inelastic vibrational features are broadened to imperceptibility, and the inelastic electronic transitions are difficult to identify because of their integral shape.[29,44] Thus, while the inelastic features disappear from the d*I*/d*V* spectrum at room temperature, the elastic tunneling OMT bands are readily observed in d*I*/d*V* spectra in the STM environment at room temperature.

Tunnel Junction IETS and OMTS. Figure 10 displays the tunnel junction NTI−*V* spectra of CoTPP. The origin of the sample bias has been shifted to give *x*-axis values of energy below the vacuum level. Note that zero bias for the tunnel junction (ϕ = 4.3 V) is at +0.9 V relative to zero bias for the Au(111) (ϕ = 5.2 V). This spectrum was acquired at 4 K, and several vibrational bands of the CoTPP are easily observed, as are their bias polarity symmetry and their appearance as well-defined peaks. Two differential-like OMTS bands are also observed, one with center near 3.4 eV and another near 5.2 eV below the vacuum level (+0.95 and −0.8 V relative to E_F of Pb). The limits on the range of data were imposed by the stability of the tunnel junction—wider scan ranges tended to destroy the devices.

Figure 11 displays the 77 K tunnel junction NTI−*V* spectra of NiTPP. As in Figure 10, the data have been shifted to provide values of energy below the vacuum level. At 77 K, all the vibrational features are lost to thermal broadening, and only

(40) Hamers, R. J. *J. Phys. Chem.* **1996**, *100*, 13103−13120.
(41) If the electroactive layer is thick or separated from both electrodes, this is not the case. See, for example: Sumi, H. *J. Phys. Chem. B* **1998**, *102*, 1833−1844. See also ref 13.
(42) Snyder, S. R.; White, H. S. *J. Electroanal. Chem.* **1995**, *394*, 177−185.
(43) *CRC Handbook of Chemistry and Physics*, 68th ed., E89−90; CRC Press: Boca Raton, FL, 1988.
(44) Hipps, K. W.; Susan, L. P. *J. Phys. Chem.* **1989**, *93*, 5717−5721.

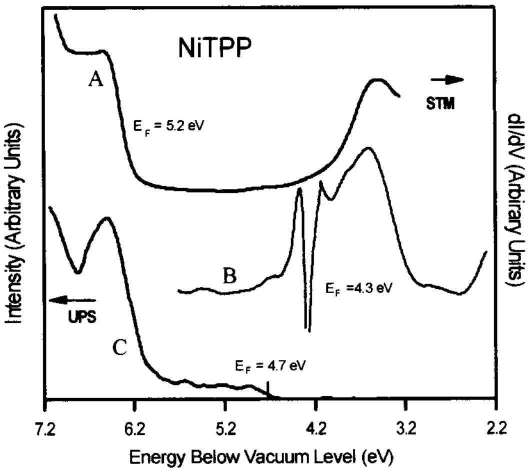

Figure 11. Combined results of UPS, STM d*I*/d*V* OMTS, and tunnel junction combined IETS and OMTS of NiTPP thin films. Curve positions on the *x*-axis are adjusted for differences in device work function. Trace A gives the STM d*I*/d*V* data. These were acquired from a 0.1 nm thick NiTPP film on Au(111) using a PtIr tip at a fixed height consistent with 0.1 nA and 0.3 V bias. B is the NTI−*V* spectrum from an Al−Al_2O_3−NiTPP−Pb junction taken at 77 K, and C is the smoothed ultraviolet photoelectron spectrum of a 4 nm film on polycrystalline gold.

the intense electronic features can be observed. The OMTS of NiTPP in an [Al−Al_2O_3−NiTPP−Pb] junction shows only one strong derivative-like band with center near 3.35 V below the vacuum state (+1.0 V relative to E_F of Pb). Unlike the CoTPP case, NiTPP has no OMTS band in the accessible negative bias region (energies between 4.3 and 5.7 V below the vacuum level).

These data are very similar to results obtained by Mazur et al. for metallophthalocyanines (MPc's),[30] where an electrochemical model was used to estimate the positions of the lowest unoccupied π^* and highest occupied d_{z^2} MOs. They assigned the positive bias OMT band in a series of MPc's as due to electron injection into the π^* LUMO. CoPc and NiPc negative bias spectra are distinctly different.[30] The CoPc has an OMTS band in the negative bias region, while the NiPc does not. This is as expected on the basis of the oxidation potentials of these ions. Thus, the first oxidation feature was assigned to the Co(II) → Co(III) + e^- process. On the basis of the similarity of spectra and electrochemistry of MPc and MTPP complexes, we assign the OMTS band in CoTPP near 3.4 eV below the vacuum level as due to the transient reduction of the LUMO π^* orbital and the 5.2 eV band as due to the transient oxidation of the half-filled HOMO of d_{z^2} orbital type.

STM−OMTS. Also shown in Figures 10 and 11 are the OMT spectra in d*I*/d*V* form acquired in the STM environment. Energies are reported as values below the vacuum level by using the measured Au work function of 5.2 eV. The STM−OMTS of CoTPP (Figure 10) has several interesting features. When the sample is biased positive (+1.7 V bias) there is a well-defined peak, corresponding to an unoccupied orbital at an electron affinity of 3.5 eV. There is a weaker but well-defined peak at 5.3 eV below the vacuum level (near −0.1 V bias), a strong peak near 6.4 eV (−1.2 V bias), and a strong shoulder at more negative bias, all corresponding to occupied orbitals. The OMTS bands of CoTPP seen in the tunnel junction are, remarkably, in nearly the same positions as those seen in the STM.

The STM orbital-mediated tunneling spectrum of NiTPP seen in Figure 11 is simpler than that of CoTPP, and the positions of oxidation and reduction peaks are given in Table 2. While an unoccupied orbital is seen near 3.5 V below the vacuum level and an occupied orbital occurs at 6.5 V with an increasing signal at larger voltages, the band near 5.3 V is absent. Thus, following the tunnel junction OMTS assignments, we identify the first affinity level (3.5 eV below the vacuum level) as due to the LUMO π^* orbital and the first ionization energy of CoTPP near 5.3 eV as due to ionization from the half-filled d_{z^2} orbital. In both the NiTPP and CoTPP cases, we attribute the strong band associated with an ionization energy of about 6.5 eV to π ring oxidation.

Table 2. Ring and Metal Orbital Energies (below the Vacuum Level) As Observed by STM−OMTS and Electrochemical Model Predictions

compound	method	first ring oxidation	first metal oxidation	first ring reduction
NiTPP	STM OMTS	6.5	A1RO[a]	3.5
CoTPP	STM OMTS	6.4	5.3	3.5
CoTPP	electrochemical[b]	5.8	5.0	2.9
NiTPP	electrochemical[b]	5.8	A1RO[a]	3.5
ZnTPP	electrochemical[b]	5.4	A1RO[a]	3.4
H_2TPP	electrochemical[b]	5.7		3.7
CdTPP	electrochemical[b]	5.3		3.5

[a] A1RO = above (more positive than) or near the first ring oxidation. [b] Electrochemical values taken from ref 47. 0.0 V SCE was taken to be 4.7 V relative to the vacuum level.[27]

This last assignment is significantly strengthened by plotting the smoothed UPS spectra of the appropriate compounds in Figures 10 and 11. Curves A and C of Figures 10 and 11 are in excellent agreement and allow assignment of the band near 6.5 eV ionization energy as due to the two highest occupied porphyrin ring orbitals, the $a_{1u}(\pi)$ and $a_{2u}(\pi)$ MOs.

In previous publications we have used an electrochemical model to estimate the positions of OMTS bands.[30,45,46] We found that the reduction potentials closely correlated with the first (positive bias) OMTS bands in a number of compounds. We also observed that metal-centered oxidation generally differed from the predicted values by a few tenths of a volt. This was a small discrepancy that we associated with solvent coordination in solution. The STM−OMTS data presented in this paper offers an especially rich opportunity to test that model since we observe both oxidation and reduction potentials spread over about 3 V in potential. In our model, the ionization energies and electron affinities of thin films supported on metals should be approximately given by the first electrochemical oxidation and reduction potentials, respectively.[30] To convert potential relative to SCE to values referenced to the vacuum level, we add 4.7 V to the electrochemical values as shown in Figure 2.[27] Table 2 contrasts the STM−OMTS observed peak positions with the electrochemical values for several metalloporphyrins.[47] Consider first the values obtained for the first ring reduction potential. With the exception of the CoTPP electrochemical value (which we discount because it is not consistent with the results for other metalloporphyrins), STM−OMTS and electrochemical reduction potentials are in good agreement. The CoTPP d_{z^2} oxidation potential is about 0.3 V deeper than the electrochemical value. This is not surprising in the context of the availability of the half-filled d_{z^2} orbital axial solvent interaction. The first ring oxidation, however, is almost 0.8 V deeper in the adsorbed film than in solution. This is a large error that cannot be easily explained. Thus, it appears that the electrochemical model is

(45) Mazur, U.; Hipps, K. W. *J. Phys. Chem.* **1995**, *99*, 6684−6688.
(46) Hipps, K. W.; Barlow, D. E.; Mazur, U. *J. Phys. Chem. B* **2000**, *104*, 2444−2447.
(47) *The Porphyrins Physical Chemistry: Part C*; Dolphin, D., Ed.; Academic Press: New York, 1978; pp 142−144.

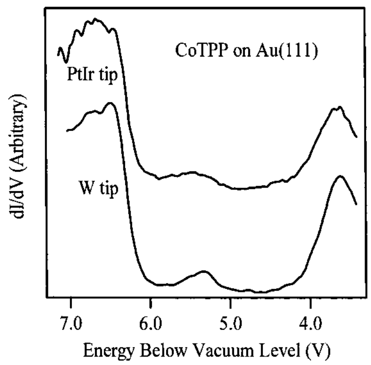

Figure 12. Comparison of STM d*I*/d*V* spectra of CoTPP on Au(111) as obtained with PtIr (0.3 V, 0.1 nA) and W (0.3V, 0.3 nA) tips.

more appropriate for estimating electron affinity levels than for ionization energies.

We comment here on the voltage region used for STM OMTS studies. It is very easy to cause gold atom and/or adsorbate migration and even severe field emission with a biased STM tip. We have found that the *I*−*V* curves become unstable and irreproducible when voltage scans greater than about ±2.4 V are used. In fact, depending on the extent of coverage by the adsorbate, the quality of the tip, and the relative number of surface defects, smaller scan ranges are sometimes required.

Tip Material Dependence. The work functions of polycrystalline W (∼4.6 eV) and Pt (∼5.6 eV) differ by about 1 eV.[36] Moreover, the work function of W is lower than that of Au(111), while that of Pt is greater. Thus, we would expect the Au−W and Au−PtIr "junctions" formed in the STM to have a significant internal field and to differ in polarity. One asks, therefore, if these differences affect the positions of bands observed in OMT spectroscopy. To answer this question as it relates to the results reported here, we measured d*I*/d*V* spectra of the same CoTPP-on-Au(111) sample with both W and PtIr tips. Figure 12 contrasts the spectra obtained with W and with Pt−Ir tips. Within the accuracy of the measurements, there are no significant shifts in peak position despite the 1 V difference in internal potential expected. The spectra acquired with the Pt−Ir tip appear broader, but that may be due to some peculiarity of the tip shape. It will require comparisons of many different tips of both types to determine if line width effects are produced by tip material changes. We note here that Tao[14] measured the apparent heights of protoporphyrin complexes adsorbed on gold in an electrochemical STM and found that the height versus substrate potential at fixed substrate−tip bias was also independent of the tip materials.

If the adsorbate layer is thin compared to the tip−substrate gap, we would expect the internal potential created by the tip−substrate work function difference to have relatively little effect on the positions of the adsorbate electronic energy levels. On the other hand, if the entire tip−substrate gap is filled with adsorbate material, we would expect to see significant changes in peak positions and line widths with changes in tip−substrate work function changes. This issue will be addressed in future experiments wherein varying thickness MTPP layers, changes in tip material, and systematic changes in tip height (through initial bias and setpoint settings) will be explored.

Conclusions

Thin films of CoTPP and NiTPP were studied by UPS, STM imaging, STM d*I*/d*V* spectroscopy, and NTI−*V* spectroscopy in the tunnel junction configuration. The ultraviolet photoelectron spectrum gives the position of the highest occupied π MOs but does not reveal the location of the highest lying half-filled MO in CoTPP, the d_{z^2} orbital. In the [Al−Al_2O_3−MTPP−Pb] tunnel junctions, the lowest unoccupied π^* orbital (for both Ni(II) and Co(II)) and the highest energy occupied MO (d_{z^2}) (in Co(II)) were observed as orbital-mediated tunneling bands. In the STM environment, π (for NiTPP and CoTPP) and d_{z^2} (in CoTPP) high-energy occupied orbitals and the lowest energy unoccupied π^* orbital were all observed. Thus, in the region of the Fermi energy, STM−OMTS allows the determination of both filled and unfilled orbitals and in general has more information than either UPS or tunnel junction-based OMTS. It appears that a previously proposed electrochemical model is more appropriate for estimating electron affinity levels than for ionization energies. The present work is the first report of the observation of STM−OMTS, tunnel junction OMTS, and UPS of the same compounds.

Acknowledgment. We thank the National Science foundation for support in the form of Grants CHE 9709273 and CHE 9819318. Acknowledgment is also made to the donors of the Petroleum Research Fund, administered by the ACS, and to Research Corporation for partial support of this research.

JA0100726